

Measurement report: Comparison of wintertime individual particles at ground level and above the mixed layer in urban Beijing

Wenhua Wang^{1,2,3}, Longyi Shao^{1*}, Claudio Mazzoleni³, Yaowei Li¹, Simone Kotthaus⁴, Sue Grimmond⁴,
Janarjan Bhandari³, Jiaoping Xing^{1,5}, Xiaolei Feng¹, Mengyuan Zhang¹, Zongbo Shi⁶

1. State Key Laboratory of Coal Resources and Safe Mining & College of Geosciences and Surveying Engineering, China University of Mining and Technology, Beijing, 100083, China

2. School of Resources and Materials, Northeastern University at Qinhuangdao, Qinhuangdao, 066004, China

3. Atmospheric Sciences Program & Physics Department, Michigan Technological University, Houghton, 49931, USA

4. Department of Meteorology, University of Reading, Reading, RG6 6BB, UK

5. School of Forestry, Jiangxi Agricultural University, Nanchang, 330045, China

6. School of Geography Earth and Environmental Sciences, the University of Birmingham, Birmingham, B15 2TT, UK

* Corresponding author: ShaoL@cumtb.edu.cn

Abstract:

Beijing has been suffering from frequent severe air pollution events, with concentrations affected significantly by the mixed layer height. Major efforts have been made to study the physico-chemical properties, compositions, and sources of aerosol particles at ground level. However, little is known about the morphology, elemental composition, and mixing state of aerosol particles above the mixed layer. In this work, we collected individual aerosol particles simultaneously at ground level (2 m above ground) and above the mixed layer in urban Beijing (within the Atmospheric Pollution and Human Health in a Chinese Megacity (APHH-Beijing) 2016 winter campaign). The particles were analyzed off-line by transmission electron microscopy coupled with energy dispersive X-ray spectroscopy. Our results showed that the relative number contribution of mineral particles to all measured particles was much higher during non-haze periods (42.5%) than haze periods (18.1%); on the contrary, internally mixed particles contributed more during haze periods (21.9%) than non-haze periods (7.2%) at ground level. In addition, more mineral particles were found at ground level than above the mixed layer height. Around 20% of individual particles showed core-shell structures during haze periods, whereas only a few core-shell particles were observed during non-haze periods (2%). The results showed that the particles above the mixed layer were more aged with a larger proportion of organic particles originated from coal combustion. Our results indicate that a large fraction of the airborne particles above the mixed layer come from surrounding areas influenced by coal combustion activities. This source contributes to the surface particle concentrations in Beijing when polluted air is mixed down to the ground level.

Keywords: haze; individual particle; organic particle; core-shell structure; mixed layer.

34 1. Introduction

35 Atmospheric aerosols emitted from anthropogenic or natural sources are composed of a variety
36 of chemical components (e.g., organic matter, black carbon, nitrate, sulfate, ammonium, metals,
37 mineral dust) (Merikallio et al., 2011; Guo et al., 2014; Wang et al., 2016; Peng et al., 2016; Shao et
38 al., 2017; Tao et al., 2017). Anthropogenic aerosols have received increasing attention in recent
39 decades due to their effects on climate and the environment. In fact, anthropogenic aerosols affect
40 climate through cloud condensation nuclei activity (Kerminen et al., 2012), hygroscopic growth
41 (Brock et al., 2016), and light scattering and absorption (Jacobson, 2001; Bond and Bergstrom, 2006;
42 Merikallio et al., 2011; China et al., 2013; Peng et al., 2016; Bhandari et al., 2019b). They can also
43 have adverse effects on human health, for example, by carrying toxic and carcinogenic compounds
44 (Chen et al., 2013; Shao et al., 2016, 2017). High concentrations of aerosol particles in urban air
45 can cause cardiovascular, respiratory, and even nervous system diseases (Xia et al., 2018; De Marco
46 et al., 2019; Shou et al., 2019). It is suggested that outdoor air pollution causes 3.3 million people
47 premature deaths worldwide each year (Lelieveld et al., 2015). Atmospheric aerosol particles also
48 affect regional and global geochemical cycles as they are transported over long distances (Heald et
49 al., 2006; Weijun Li et al., 2017; Rodriguez-Navarro et al., 2018).

50 Recently, China has suffered from severe air pollution conditions, like other countries
51 undergoing rapid social and economic development (Huang et al., 2014). In China, urban air
52 pollution is characterized by frequent occurrence of haze events, high PM_{2.5} mass level, and
53 expanded haze areas (Guo et al., 2014; Huang et al., 2014; Sun et al., 2014). For example, the
54 maximum hourly average PM_{2.5} mass concentrations in winter in Beijing reached more than 1000
55 $\mu\text{g m}^{-3}$ (Li et al., 2017a; Zhang et al., 2017), 40 times above the safe level of 25 $\mu\text{g m}^{-3}$ recommended
56 by the World Health Organization (WHO).

57 As the megacity capital, Beijing has received much attention being one of the most polluted
58 cities in China. Atmospheric researchers have been studying aerosol particles to understand haze
59 formation in China (Sun et al., 2013; Huang et al., 2014; Zhou et al., 2018b). Measurements and
60 model analyses highlight the key roles of secondary aerosol formation by trace gases (e.g., volatile
61 organic compounds, and SO₂, NO_x) and stagnant meteorological conditions in the regional haze
62 formation (Wang et al., 2013; Guo et al., 2014; Huang et al., 2014).

63 Because the characterization of aerosol particles is mainly focused on surface level
64 observations, the understanding of aerosol properties at higher altitudes in urban areas is still
65 insufficient (Zhou et al., 2018a). Vertical differences between precursors, oxidants and temperature
66 gradients might influence gas-particle partitioning and heterogeneous reactions of N_2O_5 (Zhou et
67 al., 2018a). Previous measurements at the Institute of Atmospheric Physics (IAP) meteorological
68 tower in Beijing showed complex vertical distributions of particulate matter and gaseous pollutants
69 (Meng et al., 2008; Sun et al., 2015; Wang et al., 2018; Zhou et al., 2018b). However, most of these
70 studies focused on non-refractory submicron species. Research showed that the mixed layer height
71 (MLH) could explain some of the vertical difference of aerosol particle chemical composition (Sun
72 et al., 2015; Wang et al., 2018; Zhang et al., 2012). For example, vertical distributions of aerosol
73 particles were more uniform during periods with higher MLH (Wang et al., 2018). As heavily
74 increased air pollution could reduce boundary layer heights by diminishing incoming solar energy
75 and therefore by weakening vertical turbulence, near-surface aerosol concentrations become
76 elevated (Petaja et al., 2016). Moreover, the upper layer particles could influence those below the
77 MLH by downward entrainment or mixing plumes, making the lower layer particles more complex
78 (Wehner et al., 2010; Platis et al., 2015; Qi et al., 2019). Previous studies showed that the particles
79 above the MLH considerably influenced cloud formation (Carnerero et al., 2018) and showed strong
80 aerosol-radiation effect (Bond and Bergstrom, 2006). The differences in aerosol types at ground
81 level and at higher altitudes could lead to large differences in aerosol direct forcing estimates
82 (Ramanathan et al., 2002; Li et al., 2010). The vertical difference of aerosol particles also increases
83 the uncertainties in the assessment of the climate system (Li et al., 2017b). Therefore, a detailed
84 knowledge of the vertical distribution and chemical composition of aerosols is important for
85 understanding the impact on climate and the aerosol evolution process (Zhang et al., 2009; Wang et
86 al., 2018).

87 Vertical comparisons of individual aerosol particles and their morphologies, mixing states, and
88 elemental compositions are very limited. Transmission Electron Microscopy (TEM) can provide
89 detailed individual particle characterization and help to explain heterogeneous reactions and aging
90 process (Li et al., 2016a). In this study, we compare particles simultaneously collected at ground
91 level and above the MLH based on the meteorological tower at IAP in Beijing, as part of the UK-

92 CHINA atmospheric pollution and Human Health (APHH) 2016 winter campaign.

93 **2. Experimental**

94 **2.1. Aerosol sampling**

95 Individual aerosol samples were collected at the tower division of IAP, Chinese Academy of
96 Science (39°58'N, 116°22'E), in Beijing from 1 to 9 December of 2016. The site, located between
97 the north 3rd and 4th ring roads in Beijing, is influenced by surrounding and regional traffic, and
98 commercial, as well as, residential activities (Sun et al., 2016). There is a highway 250 m East of
99 IAP.

100 Two DKL-2 single stage cascade impactors, with a 0.5-mm-diameter jet nozzle and a flow rate
101 of 1 L min⁻¹ were used. The sampler collection efficiency is ~ 100% at an aerodynamic diameter of
102 0.5 μm if the particle density is 2 g·cm⁻³ (Li et al., 2016b). Copper (Cu) TEM grids, coated with
103 carbon film (300-mesh; Tianld Co.; Beijing, China), were used to collect the aerosol samples. The
104 sampling duration varied from 30 seconds to less than 5 minutes depending on the air pollution load.
105 Simultaneous observations at ground level (Z1; 2 m above ground) and an elevated altitude (Z2;
106 280 m above ground) enabled us to obtain the vertical profile of the particles. The collected samples
107 were stored in a dry plastic tube and placed in an air dryer to minimize particle changes before
108 analysis.

109 Automatic Lidar and Ceilometer (ACL) observations of attenuated backscatter were conducted
110 at the site using a Vaisala CL31 sensor. Measurements were corrected to account for instrument-
111 related background and near range artefacts (Kotthaus et al., 2016). The MLH was derived from
112 profile measurements using the automatic CABAM algorithm (Kotthaus and Grimmond, 2018).
113 Since the TEM samples were collected for less than 5 minutes, the MLH at 15 min resolution was
114 used to determine whether the Z2 observations were located within the MLH or above the MLH
115 (Shi et al., 2019).

116 Samples were obtained during the periods shown (solid dots and dashed lines) in Fig. 1.
117 Detailed sample information is provided in Table 1. Other measurements including PM_{2.5}, SO₂, NO₂,
118 and O₃ mass concentrations at ground level were obtained from the Olympic Park monitor site,
119 which is the closest national air quality monitor station to IAP (~1.5 km) (Shi et al., 2019). City
120 average temperature (T) and relative humidity (RH) at ground level were obtained from the Ministry

121 of Ecology and Environment of China (<https://www.aqistudy.cn/>). In this study, the particles were
122 all collected in the morning and midnight when the MLH was the lowest and the height of the tower
123 could reach the MLH at that time.

124 **2.2. Individual particle analysis**

125 Individual particles were analyzed using a JEOL JEM-2800 TEM at an accelerating voltage of
126 200 kV. The morphology and mixing state of individual particles were determined from the TEM
127 images. Semi-quantitative elemental composition was determined using Energy Dispersive X-ray
128 Spectroscopy (EDS), by which elements heavier than Boron ($Z>5$) can be detected. Cu was not
129 included because the TEM grids were made of copper. The EDS collection duration of each
130 individual particle was about 15 s to reduce damage of particles from the electron beam. For most
131 particles, only one spectrum of each particle was collected and the spot size of beam would be
132 adjusted according to the size of the particles. Therefore, we obtained the average elemental
133 compositions of each particle. However, more than one spots per particle were collected if the
134 particles were inhomogeneous particles according to the TEM images. The aerosol particles were
135 not evenly distributed on the TEM grids; the coarser particles occurred near the center and the finer
136 particles occurred on the periphery. To ensure a representative data analysis, three or four meshes
137 from the center to the periphery were selected and analyzed. The projected areas of individual
138 particles were determined using the Image-J software (Schneider et al., 2012), which was commonly
139 used for counting and measuring the projected area of atmospheric particles acquired by electron
140 microscopes (Unga et al., 2018). First, the gray-scale images of the particles were converted into
141 binary images, in which black pixels represented the particles and white pixels represented the
142 background. The area equivalent diameters (D_{Aeq}) of the particles are calculated by the following
143 formula: $D_{Aeq} = 2 \cdot (A/\pi)^{1/2}$, where A is the projected area of the particles shown in the TEM images
144 (Bhandari et al., 2019a). Most of the particles with diameter larger than 100 nm were analyzed in
145 this study.

146 **3. Results and discussions**

147 **3.1. Mass concentration of air pollutants**

148 The temporal variations of different air pollutants and meteorological conditions at ground
149 level are shown in Fig. 1. The hourly averaged PM_{2.5} mass concentration at the Olympic Park

150 monitoring site ranged from 3 to 530 $\mu\text{g m}^{-3}$, with a sample period average of 113.3 $\mu\text{g m}^{-3}$,
151 significantly exceeding the safe level of 75 $\mu\text{g m}^{-3}$ according to the Chinese National Ambient Air
152 Quality Standard (GB3095-2012). The MLH ranged from 54 to 1496 m, with an average of 397 m.
153 The MLH showed obvious diurnal variation. The hourly mean RH ranged from 17% to 97%, with
154 a 9 day mean of 50.3%. The RH and $\text{PM}_{2.5}$ were positively correlated (correlation coefficient=0.75;
155 Fig. S1) according to the 216 groups of hourly data, suggesting that higher RH favors the formation
156 of haze (Sun et al., 2014; Wang et al., 2016). As expected, RH and temperature were negatively
157 correlated (correlation coefficient=-0.51; Fig. S2). The variation trend of SO_2 was similar to that of
158 NO_2 . However, the average concentration of NO_2 (83.2 $\mu\text{g m}^{-3}$) was nearly 5.5 times higher than
159 that of SO_2 (15.2 $\mu\text{g m}^{-3}$). The concentration of O_3 showed a different trend compared with NO_2 and
160 SO_2 (Fig. 1), with a 9 days hourly mean concentration of 20 $\mu\text{g m}^{-3}$.

161 3.2. Classification and mixing state of individual particles

162 Aerosol particles are classified using their morphologies and elemental compositions into
163 seven main types, namely: 1) primary organic aerosols (POA), 2) sulfur-rich (S-rich) particles, 3)
164 soot particles, 4) mineral particles, 5) metal particles, 6) internally mixed organic and sulfur-rich
165 particles (OP-S), and 7) other mixed particles. The detailed characteristics of each particle type are
166 shown in Table 2.

167 POA particles are mainly composed of C and O, usually with a small amount of Si, S, Cl, and
168 K. POA particles are relatively stable under the electron beam irradiation. Based on the
169 morphologies, POA particles can be further divided into spherical (Fig. 2a) and irregularly shapes
170 (Fig. 2b). They are mainly from combustion process of biomass and fossil fuel (Li et al., 2016a; Liu
171 et al., 2021).

172 S-rich particles (Figs. 2c and 2d) are mainly composed of O, S, and N, and sometimes also
173 contain some amount of K. S-rich particles are beam-sensitive and volatilize under strong beam
174 irradiation. S-rich particles generally represent secondary inorganic components (e.g., SO_4^{2+} , NO_3^-
175 and NH_4^+) (Xu et al., 2019).

176 Soot particles are mainly composed of C, minor amount of O, and sometimes Si. Soot particles
177 consist of a number of C-dominated spherical monomers less than 100 nm in diameter (Figs. 2e and
178 2f) and can be easily identified under high-resolution TEM (Buseck et al., 2014; Bhandari et al.,

179 2017). Soot particles, stable under the electron beam, show chain-like or compact morphologies in
180 the atmosphere (Sorensen et al., 2001; Adachi et al., 2007; China et al., 2013, 2015; Bhandari et al.,
181 2019a). Soot particles are mainly from incomplete combustion of biomass and fossil fuel.

182 Metal particles (Figs. 2g and 2h) and mineral particles (Fig. 2i) are stable under the beam
183 irradiation. Mineral particles are mostly irregularly shaped containing crustal elements (e.g., Si, Al,
184 Ca, Fe, Na, K, Mg, Ti, and S) in addition to O. They can be generated from windblown soil dust or
185 road dust. Metal particles are spherical or near spherical and are mainly composed of Fe, Zn, Mn,
186 Ti, and Pb. Metal particles are mainly originated from industries, coal-fired power plants, and oil
187 refineries (Xu et al., 2019) or vehicle brakes (Hou et al., 2018).

188 Internally mixed particles (Figs. 2j-p) are particles with at least two of the above components.
189 They usually show relative larger diameter. We further classify them as internally mixed organic
190 and sulfur-rich particles (OP-S) (Figs. 2j-l), and other mixed particles (Figs. 2m-p).

191 **3.3. Comparison of haze and non-haze individual particle at ground level**

192 Haze periods are defined as hourly average $PM_{2.5}$ mass concentration greater than $75 \mu g m^{-3}$
193 during collection time; the rest are defined as non-haze periods. A total of 1538 individual particles
194 among 8 samples at ground level were analyzed based on the TEM results. The relative number
195 percentage ($N(\text{type } i) / N(\text{total}) * 100$) of particles in each sample was calculated. The results are
196 provided in Table 3 and shown in Fig.3. During non-haze periods, the particles were composed of
197 mineral particles (42.5%), POA particles (21.1%), S-rich particles (20.0%), soot particles (6.4%),
198 other mixed particles (5.6%), metal particles (2.83%), and OP-S (1.6%) in descending order. During
199 haze periods, the particles were composed of POA particles (28.3%), S-rich particles (23.5%),
200 mineral particles (18.1%), OP-S (13.1%), other mixed particles (8.8%), soot particles (6.6%), and
201 metal particles (1.7%) in descending order.

202 The mineral particles are mainly from re-suspended road dust, soil dust, and construction dust
203 during non-desert transport dust episodes (Sun et al., 2006; Gao et al., 2016; Wang et al., 2017). The
204 relative number percentage of mineral particles was much higher during non-haze periods (42.5%)
205 than during haze periods (18.1%), as shown in Fig.3.

206 However, the content of mixed particles including OP-S and other mixed particles during haze
207 periods (21.9%) was much higher than during non-haze periods (7.2%), suggesting that there was

208 more secondary aerosol formation during haze periods. High secondary aerosol formation in winter
209 in Beijing during the pollution periods was also found in previous studies (Huang et al., 2014; Sun
210 et al., 2016; Li et al., 2017a). Secondary aerosol formation was expected since the RH during the
211 haze periods were relatively higher than during non-haze periods, as shown in Table 1 and Fig.1,
212 which facilitated chemical reactions of gaseous pollutants (Liu et al., 2016; Wang et al., 2016). Also,
213 the average content of POA particles and S-rich were higher during haze periods than during non-
214 haze periods.

215 **3.4. Comparison of individual particles at ground level and above the MLH**

216 A total of 1519 individual particles among 8 samples above the MLH were analyzed. The results
217 are provided in Table 3 and shown in Fig. 3. We found that the relative number percentage of mineral
218 particles at ground level was larger than that above the MLH. For example, mineral particles at
219 ground level and above the MLH during non-haze periods accounted for 42.5% and 23.2%,
220 respectively, and during haze periods the values are 18.1% and 9.5%, respectively. S-rich particles
221 during non-haze periods accounted for 20.0% at ground level, less than the value of 30.7% above
222 the MLH. However, not all the samples above the MLH during haze periods showed higher relative
223 number percentage of S-rich particles than at ground level. This might because some of the S-rich
224 particles above the MLH were mixed with other particles, forming mixed particles. Another reason
225 might be that higher relative number percentage of mixed particles diluted the relative number
226 percentage of S-rich particles. The mixed particles during haze periods accounted for 32.0% above
227 the MLH, higher than that of 21.9% at ground level. We also found that POA particles above the
228 MLH accounted for higher relative number percentage than at ground level, although there was
229 some variance. For example, samples 4 and 6 showed higher relative number percentage of POA
230 particles at ground level. That might because that some of the POA particles were mixed with S-
231 rich particles and OP-S showed higher relative number percentage above the MLH than at ground
232 level in samples 4 and 6. Metals and soot only accounted for a few relative number percentages in
233 all samples and they didn't show much difference at ground level and above the MLH. Particles
234 above the MLH were either transported from the surrounding areas or from ground sources. In both
235 cases, they were subject to atmospheric process, leading to their aging.

236 **3.5. Aging of particles**

237 In the atmosphere, particles are subjected to aging process. During the aging process of aerosol
238 particles, secondary species can coat pre-existing particles (Li and Shao, 2009; Laskin et al., 2016;
239 Li et al., 2016b; Niu et al., 2016; Tang et al., 2016; Chen et al., 2017; Hou et al., 2018; Unga et al.,
240 2018; Xu et al., 2019). Using high-resolution TEM images, it is possible to identify the core-shell
241 structure of particles (Li et al., 2016a). For example, Figs. 4a and 4b showed S-rich particles coated
242 by secondary species. Figs. 4c and 4d were POA particles coated with secondary species. Figs. 4e-
243 h showed core-shell structured particles with some mixed particle cores. In this study, we found that
244 the core-shell structured particles accounted for 20% during haze periods with 17% at ground level
245 and 23% above the MLH, but only 2% during non-haze periods. These results demonstrated a
246 general trend that the core-shell structured particles during haze periods were much higher than
247 during non-haze periods. Also, the average D_{Aeq} of particles was larger during haze periods than
248 during non-haze periods as shown in Fig. S3. These results confirmed that particles during haze
249 periods underwent more extensive aging than during non-haze periods.

250 The coating of atmospheric particles is often caused by aging mechanisms such as coagulation,
251 condensation, and heterogeneous chemical reactions (Kahnert, 2015; Müller et al., 2017, Zhang et
252 al., 2012). Fig. 5 shows low magnification images of particles at ground level and above the MLH.
253 More core-shell particles were found above the MLH. The core/shell ratio (R), which is the ratio of
254 the D_{Aeq} of core to the D_{Aeq} of whole particle including the coating, has been used to evaluate the
255 aging process of aerosol particles in different studies (Niu et al., 2012, 2016; Hou et al., 2018). The
256 value of R ranged from 0 to less than 1. A smaller R value means the particles are more coated, thus
257 are subjected to a more extensive degree of aging (Hou et al., 2018). Because high number
258 percentage of core-shell structured particles were only found during haze periods, we only measured
259 R of core-shell structured particles during the haze periods (including the samples 2, 4, 5, 6 and 7).
260 Fig. 6a shows the R value of each samples during the haze periods. We can see from Fig. 6a that all
261 the samples showed a smaller average R value above the MLH compared with those from the ground
262 level. The average R value above the MLH (0.54) was smaller than ground level (0.59). Additionally,
263 the relative number percentage of core-shell structured particles was higher above the MLH than at
264 ground level, except for sample 4. These findings indicated that the particles above the MLH were
265 more aged than those at ground level.

266 Fig. S3 shows the total particle number-size distribution; the relative number percentage of the
267 larger size particles clearly increased when considering the coatings compared to only considering
268 the core size during haze periods. The change in optical properties due to coating was calculated in
269 various studies by using different methods (Cappa et al., 2012; Scarnato et al., 2013; Liu et al., 2015;
270 Saliba et al., 2016; Unga et al., 2018). When host particles were coated, their optical properties
271 might be amplified (Khalizov et al., 2009; Peng et al., 2016). Also, organic coating can influence
272 the hygroscopic properties and the viscosity of mixed particles (Sharma et al., 2018; Unga et al.,
273 2018), and thus can influence cloud formation activity (Kerminen et al., 2012).

274 **3.6. Possible sources of organic particles**

275 Our results showed higher relative number percentage of POA particles both during non-haze
276 (21.1%) and haze periods (28.3%) in winter Beijing, compared with a tunnel environment (~5%),
277 where the vehicle emissions were the main pollution sources (Hou et al., 2018). Also, recent studies
278 did not find abundant POA particles in North China during Spring and Summer (Yuan et al., 2015;
279 Li et al., 2016b; Xu et al., 2019;). Instead, a larger number percentage of POA particles have been
280 found in winter using electron microscopy in previous studies, including an outflow of a haze plume
281 in East Asia (Zhu et al., 2013), a coal-burning region in China's Loess Plateau (Li et al., 2012), three
282 sampling sites in North China Plain (Chen et al., 2017) and urban and rural sites in Northeast China
283 (Xu et al., 2017; Zhang et al., 2017). These results suggested that POA particles accounted for a
284 large number percentage of the particles in north China in winter.

285 Most of the POA particles in our study were spherical or nearly spherical in shape according
286 to the projected images and they were stable under strong electron beam irradiation and appear dark
287 features in TEM images, which reflected their high thickness and refractory properties (Ebert et al.,
288 2016), suggesting that they were formed through cooling process after the biomass or fossil fuel
289 combustion pyrolysis products of volatile organic compounds were emitted into the atmosphere
290 (Wang et al., 2015; Chen et al., 2017; Zhang et al., 2017).

291 These spherical or near spherical POA particles are considered to be brown carbon (Zhang et
292 al., 2020). Brown carbon plays a significant role in atmospheric shortwave absorption and can cause
293 warming of the atmosphere (Adachi and Buseck, 2011; Hoffer et al., 2016). Some researchers have
294 found that the primary POA particles from coal combustion have more Si than those from biomass

295 burning (Li et al., 2012; Chen et al., 2017). The weight ratio of C-O-Si at ground level and above
296 the MLH is shown in Fig. 7. More coal burning related POA particles were found above the MLH.
297 Since the relative number percentage of POA particles affected by coal burning are higher above
298 the MLH than at ground level, POA particles above the MLH are not all from ground level and
299 might be originated from surrounding areas influenced by coal combustion. The results were
300 supported by the 24-h backward trajectories, which showed that air masses above the MLH during
301 haze periods were from the North and West direction of Beijing as shown in Fig. S4. It is reasonable
302 that Beijing has implemented strict air pollution controls measures, including using natural gas to
303 replace domestic coal burning. The particles above the MLH can contribute to Beijing air pollution
304 by mixing down to the ground.

305 4. Conclusions

306 Detailed morphologies and elemental compositions of individual aerosol particles at ground level
307 and above the mixed layer height were analyzed in this study. Following conclusions were achieved:

308 1) Particles were classified into primary organic particles, S-rich particles, mineral particles,
309 metal particles, soot, internally mixed organic and sulfur-rich particles, and other mixed particles.
310 Compared with non-haze periods, haze periods were associated with a relative lower number
311 percentage of mineral particles and a relative higher number percentage of mixed particles.

312 2) Compared with the aerosol samples at ground level, the samples above MLH had a lower
313 relative number percentage of mineral particles, a higher number percentage of coated particles, a
314 smaller core/shell ratio of coated particles. More coated particles and higher core/shell ratio in the
315 aerosol samples above the mixed layer suggested that the particles above the mixed layer were more
316 aged.

317 3) Relative number percentage of primary organic particles accounted for 21.1% during non-haze
318 periods and 28.3% during haze periods in winter Beijing. More primary organic particles above the
319 mixed layer were associated with coal combustion according to the C-O-Si ratio, and the long-range
320 transportation of air masses from surrounding areas has an important influence for Beijing air.

321 **Data availability:** Data used in this study are available from the corresponding author upon request
322 (ShaoL@cumtb.edu.cn)

323 **Author Contributions:** WW, LS, CM, JX and ZS conceived the manuscript. WW, WL, XF and
324 MZ conducted the sample collection and analysis. SK and SG conducted the MLH measurement.
325 CM and BJ conducted manuscript modification.

326 **Competing interest:** The authors declare no conflict of interest.

327 **Acknowledgements:** We thank Zifa Wang and Pingqing Fu at IAP for the supporting of sample
328 collection. This work was supported by National Natural Science Foundation of China (No.
329 42075107), International Cooperation Projects of National Natural Science Foundation of China
330 (No. 41571130031), China Scholarship Council (No. 201806430015), Yue Qi Scholar Fund of
331 China University of Mining and Technology (Beijing). CM and JB were supported by the U.S
332 Department of Energy (DOE), Office of Biological and Environmental Research (OBER),
333 Atmospheric System Research (#DE-SC0011935 and Grant # DE-SC0018931). ZS was supported
334 by Natural Environmental Research Council (NE/N007190/1).

335 **Reference:**

- 336 Adachi, K., Chung, S. H., Friedrich, H., and Buseck, P. R.: Fractal parameters of individual soot particles
337 determined using electron tomography: Implications for optical properties, *Journal of Geophysical*
338 *Research*, 112, 10.1029/2006jd008296, 2007.
- 339 Adachi, K., and Buseck, P. R.: Atmospheric tar balls from biomass burning in Mexico, *J. Geophys. Res.-*
340 *Atmos.*, 116, 7, 10.1029/2010jd015102, 2011.
- 341 Bhandari, J., China, S., Onasch, T., Wolff, L., Lambe, A., Davidovits, P., Cross, E., Ahern, A., Olfert, J., Dubey,
342 M., and Mazzoleni, C.: Effect of Thermodenuding on the Structure of Nascent Flame Soot Aggregates,
343 *Atmosphere*, 8, 10.3390/atmos8090166, 2017.
- 344 Bhandari, J., China, S., Chandrakar, K. K., Kinney, G., Cantrell, W., Shaw, R. A., Mazzoleni, L. R., Girotto,
345 G., Sharma, N., Gorkowski, K., Gilardoni, S., Decesari, S., Facchini, M. C., Zanca, N., Pavese, G., Esposito,
346 F., Dubey, M. K., Aiken, A. C., Chakrabarty, R. K., Moosmuller, H., Onasch, T. B., Zaveri, R. A., Scarnato, B.
347 V., Fialho, P., and Mazzoleni, C.: Extensive Soot Compaction by Cloud Processing from Laboratory and
348 Field Observations, *Sci Rep*, 9, 11824, 10.1038/s41598-019-48143-y, 2019a.
- 349 Bhandari, J., China, S., Girotto, G., Scarnato, B. V., Gorkowski, K., Aiken, A. C., Dubey, M. K., and Mazzoleni,
350 C.: Optical properties and radiative forcing of fractal-like tar ball aggregates from biomass burning,
351 *Journal of Quantitative Spectroscopy and Radiative Transfer*, 230, 65-74, 10.1016/j.jqsrt.2019.01.032,
352 2019b.
- 353 Bond, T. C., and Bergstrom, R. W.: Light Absorption by Carbonaceous Particles: An Investigative Review,
354 *Aerosol Science and Technology*, 40, 27-67, 10.1080/02786820500421521, 2006.
- 355 Brock, C. A., Wagner, N. L., Anderson, B. E., Attwood, A. R., Beyersdorf, A., Campuzano-Jost, P., Carlton,
356 A. G., Day, D. A., Diskin, G. S., Gordon, T. D., Jimenez, J. L., Lack, D. A., Liao, J., Markovic, M. Z.,
357 Middlebrook, A. M., Ng, N. L., Perring, A. E., Richardson, M. S., Schwarz, J. P., Washenfelder, R. A., Welti,
358 A., Xu, L., Ziemba, L. D., and Murphy, D. M.: Aerosol optical properties in the southeastern United States
359 in summer – Part 1: Hygroscopic growth, *Atmospheric Chemistry and Physics*, 16, 4987-
360 5007, 10.5194/acp-16-4987-2016, 2016.
- 361 Buseck, P. R., Adachi, K., Gelencsér, A., Tompa, É., and Pósfai, M.: Ns-Soot: A Material-Based Term for
362 Strongly Light-Absorbing Carbonaceous Particles, *Aerosol Science and Technology*, 48, 777-788,
363 10.1080/02786826.2014.919374, 2014.
- 364 Cappa, C. D., Onasch, T. B., Massoli, P., Worsnop, D. R., Bates, T. S., Cross, E. S., Davidovits, P., Hakala, J.,
365 Hayden, K. L., Jobson, B. T., Kolesar, K. R., Lack, D. A., Lerner, B. M., Li, S.-M., Mellon, D., Nuaaman, I.,
366 Olfert, J. S., Petäjä, T., Quinn, P. K., Song, C., Subramanian, R., Williams, E. J., and Zaveri, R. A.: Radiative
367 Absorption Enhancements Due to the Mixing State of Atmospheric Black Carbon, *Science*, 337, 1078,
368 10.1126/science.1223447, 2012.
- 369 Carnerero, C., Pérez, N., Reche, C., Ealo, M., Titos, G., Lee, H.-K., Eun, H.-R., Park, Y.-H., Dada, L., Paasonen,
370 P., Kerminen, V.-M., Mantilla, E., Escudero, M., Gómez-Moreno, F. J., Alonso-Blanco, E., Coz, E., Saiz-
371 Lopez, A., Temime-Roussel, B., Marchand, N., Beddows, D. C. S., Harrison, R. M., Petäjä, T., Kulmala, M.,
372 Ahn, K.-H., Alastuey, A., and Querol, X.: Vertical and horizontal distribution of regional new particle
373 formation events in Madrid, *Atmospheric Chemistry and Physics*, 18, 16601-16618, 10.5194/acp-18-

374 16601-2018, 2018.

375 Chen, S., Xu, L., Zhang, Y., Chen, B., Wang, X., Zhang, X., Zheng, M., Chen, J., Wang, W., Sun, Y., Fu, P.,
376 Wang, Z., and Li, W.: Direct observations of organic aerosols in common wintertime hazes in North China:
377 insights into direct emissions from Chinese residential stoves, *Atmospheric Chemistry and Physics*, 17,
378 1259-1270, 10.5194/acp-17-1259-2017, 2017.

379 Chen, Y., Ebenstein, A., Greenstone, M., and Li, H.: Evidence on the impact of sustained exposure to air
380 pollution on life expectancy from China's Huai River policy, *Proc Natl Acad Sci U S A*, 110, 12936-12941,
381 10.1073/pnas.1300018110, 2013.

382 China, S., Mazzoleni, C., Gorkowski, K., Aiken, A. C., and Dubey, M. K.: Morphology and mixing state of
383 individual freshly emitted wildfire carbonaceous particles, *Nat Commun*, 4, 2122,
384 10.1038/ncomms3122, 2013.

385 China, S., Mazzoleni, C., Gorkowski, K., Aiken, A.C. and Dubey, M.K., 2013. Morphology and mixing state
386 of individual freshly emitted wildfire carbonaceous particles. *Nat Commun*, 4: 2122.

387 China, S., Scarnato, B., Owen, R. C., Zhang, B., Ampadu, M. T., Kumar, S., Dzepina, K., Dziobak, M. P.,
388 Fialho, P., Perlinger, J. A., Hueber, J., Helmig, D., Mazzoleni, L. R., and Mazzoleni, C.: Morphology and
389 mixing state of aged soot particles at a remote marine free troposphere site: Implications for optical
390 properties, *Geophysical Research Letters*, 42, 1243-1250, 10.1002/2014gl062404, 2015.

391 De Marco, A., Proietti, C., Anav, A., Ciancarella, L., D'Elia, I., Fares, S., Fornasier, M. F., Fusaro, L., Gualtieri,
392 M., Manes, F., Marchetto, A., Mircea, M., Paoletti, E., Piersanti, A., Rogora, M., Salvati, L., Salvatori, E.,
393 Screpanti, A., Vialetto, G., Vitale, M., and Leonardi, C.: Impacts of air pollution on human and ecosystem
394 health, and implications for the National Emission Ceilings Directive: Insights from Italy, *Environ Int*, 125,
395 320-333, 10.1016/j.envint.2019.01.064, 2019.

396 Ebert, M., Weigel, R., Kandler, K., Günther, G., Molleker, S., Groß, J. U., Vogel, B., Weinbruch, S., and
397 Borrmann, S.: Chemical analysis of refractory stratospheric aerosol particles collected within the arctic
398 vortex and inside polar stratospheric clouds, *Atmos. Chem. Phys.*, 16, 8405-8421, 10.5194/acp-16-
399 8405-2016, 2016.

400 Gao, J., Peng, X., Chen, G., Xu, J., Shi, G. L., Zhang, Y. C., and Feng, Y. C.: Insights into the chemical
401 characterization and sources of PM(2.5) in Beijing at a 1-h time resolution, *Sci Total Environ*, 542, 162-
402 171, 10.1016/j.scitotenv.2015.10.082, 2016.

403 Guo, S., Hu, M., Zamora, M. L., Peng, J., Shang, D., Zheng, J., Du, Z., Wu, Z., Shao, M., Zeng, L., Molina,
404 M. J., and Zhang, R.: Elucidating severe urban haze formation in China, *Proc Natl Acad Sci U S A*, 111,
405 17373-17378, 10.1073/pnas.1419604111, 2014.

406 Heald, C. L., Jacob, D. J., Park, R. J., Alexander, B., Fairlie, T. D., Yantosca, R. M., and Chu, D. A.: Transpacific
407 transport of Asian anthropogenic aerosols and its impact on surface air quality in the United States,
408 *Journal of Geophysical Research*, 111, 10.1029/2005jd006847, 2006.

409 Hoffer, A., Toth, A., Nyiro-Kosa, I., Posfai, M., and Gelencser, A.: Light absorption properties of
410 laboratory-generated tar ball particles, *Atmospheric Chemistry and Physics*, 16, 239-246, 10.5194/acp-
411 16-239-2016, 2016.

412 Hou, C., Shao, L., Hu, W., Zhang, D., Zhao, C., Xing, J., Huang, X., and Hu, M.: Characteristics and aging of
413 traffic-derived particles in a highway tunnel at a coastal city in southern China, *Sci Total Environ*, 619-
414 620, 1385-1393, 10.1016/j.scitotenv.2017.11.165, 2018.

415 Huang, R. J., Zhang, Y., Bozzetti, C., Ho, K. F., Cao, J. J., Han, Y., Daellenbach, K. R., Slowik, J. G., Platt, S.
416 M., Canonaco, F., Zotter, P., Wolf, R., Pieber, S. M., Bruns, E. A., Crippa, M., Ciarelli, G., Piazzalunga, A.,
417 Schwikowski, M., Abbaszade, G., Schnelle-Kreis, J., Zimmermann, R., An, Z., Szidat, S., Baltensperger, U.,
418 El Haddad, I., and Prevot, A. S.: High secondary aerosol contribution to particulate pollution during haze
419 events in China, *Nature*, 514, 218-222, 10.1038/nature13774, 2014.

420 Jacobson, M. Z.: Strong radiative heating due to the mixing state of black carbon in atmospheric aerosols,
421 *Nature*, 409, 695-697, 10.1038/35055518, 2001.

422 Kahnert, M.: Modelling radiometric properties of inhomogeneous mineral dust particles: Applicability
423 and limitations of effective medium theories, *Journal of Quantitative Spectroscopy and Radiative*
424 *Transfer*, 152, 16-27, 10.1016/j.jqsrt.2014.10.025, 2015.

425 Kerminen, V. M., Paramonov, M., Anttila, T., Riipinen, I., Fountoukis, C., Korhonen, H., Asmi, E., Laakso,
426 L., Lihavainen, H., Swietlicki, E., Svenningsson, B., Asmi, A., Pandis, S. N., Kulmala, M., and Petäjä, T.:
427 Cloud condensation nuclei production associated with atmospheric nucleation: a synthesis based on
428 existing literature and new results, *Atmospheric Chemistry and Physics*, 12, 12037-12059, 10.5194/acp-
429 12-12037-2012, 2012.

430 Khalizov, A. F., Xue, H., Wang, L., Zheng, J., and Zhang, R.: Enhanced Light Absorption and Scattering by
431 Carbon Soot Aerosol Internally Mixed with Sulfuric Acid, *The Journal of Physical Chemistry A*, 113, 1066-
432 1074, 10.1021/jp807531n, 2009.

433 Kotthaus, S., O'Connor, E., Münkel, C., Charlton-Perez, C., Haeffelin, M., Gabey, A. M., and Grimmond,
434 C. S. B.: Recommendations for processing atmospheric attenuated backscatter profiles from Vaisala
435 CL31 ceilometers, *Atmos. Meas. Tech.*, 9, 3769-3791, 10.5194/amt-9-3769-2016, 2016.

436 Kotthaus, S., and Grimmond, C. S. B.: Atmospheric boundary-layer characteristics from ceilometer
437 measurements. Part 1: A new method to track mixed layer height and classify clouds, *Quarterly Journal*
438 *of the Royal Meteorological Society*, 144, 1525-1538, 10.1002/qj.3299, 2018.

439 Laskin, A., Gilles, M. K., Knopf, D. A., Wang, B., and China, S.: Progress in the Analysis of Complex
440 Atmospheric Particles, *Annu Rev Anal Chem (Palo Alto Calif)*, 9, 117-143, 10.1146/annurev-anchem-
441 071015-041521, 2016.

442 Lelieveld, J., Evans, J. S., Fnais, M., Giannadaki, D., and Pozzer, A.: The contribution of outdoor air
443 pollution sources to premature mortality on a global scale, *Nature*, 525, 367-371, 10.1038/nature15371,
444 2015.

445 Li, J., Du, H., Wang, Z., Sun, Y., Yang, W., Li, J., Tang, X., and Fu, P.: Rapid formation of a severe regional
446 winter haze episode over a mega-city cluster on the North China Plain, *Environ Pollut*, 223, 605-615,
447 10.1016/j.envpol.2017.01.063, 2017a.

448 Li, W., and Shao, L.: Transmission electron microscopy study of aerosol particles from the brown hazes
449 in northern China, *Journal of Geophysical Research*, 114, 10.1029/2008jd011285, 2009.

450 Li, W., Shi, Z., Zhang, D., Zhang, X., Li, P., Feng, Q., Yuan, Q., and Wang, W.: Haze particles over a coal-
451 burning region in the China Loess Plateau in winter: Three flight missions in December 2010, *Journal of*
452 *Geophysical Research: Atmospheres*, 117, n/a-n/a, 10.1029/2012jd017720, 2012.

453 Li, W., Shao, L., Zhang, D., Ro, C.-U., Hu, M., Bi, X., Geng, H., Matsuki, A., Niu, H., and Chen, J.: A review
454 of single aerosol particle studies in the atmosphere of East Asia: morphology, mixing state, source, and
455 heterogeneous reactions, *Journal of Cleaner Production*, 112, 1330-1349,
456 10.1016/j.jclepro.2015.04.050, 2016a.

457 Li, W., Sun, J., Xu, L., Shi, Z., Riemer, N., Sun, Y., Fu, P., Zhang, J., Lin, Y., Wang, X., Shao, L., Chen, J., Zhang,
458 X., Wang, Z., and Wang, W.: A conceptual framework for mixing structures in individual aerosol particles,
459 *Journal of Geophysical Research: Atmospheres*, 121, 13,784-713,798, 10.1002/2016jd025252, 2016b.

460 Li, Z., Lee, K.-H., Wang, Y., Xin, J., and Hao, W.-M.: First observation-based estimates of cloud-free aerosol
461 radiative forcing across China, 115, 10.1029/2009jd013306, 2010.

462 Li, Z., Guo, J., Ding, A., Liao, H., Liu, J., Sun, Y., Wang, T., Xue, H., Zhang, H., and Zhu, B.: Aerosol and
463 boundary-layer interactions and impact on air quality, *National Science Review*, 4, 810-833,
464 10.1093/nsr/nwx117, 2017b.

465 Liu, L., Zhang, J., Zhang, Y.X., Wang, Y.Y., Xu, L., Yuan, Q., Liu, D.T., Sun, Y.L., Fu, P.Q., Shi, Z.B., and Li, W.J.:
466 Persistent residential burning-related primary organic particles during wintertime hazes in North China:
467 insights into their aging and optical changes, *Atmospheric chemistry and physics*, 21, 2251-2265,
468 10.5194/acp-21-2251-2021, 2021.

469 Liu, S., Aiken, A. C., Gorkowski, K., Dubey, M. K., Cappa, C. D., Williams, L. R., Herndon, S. C., Massoli, P.,
470 Fortner, E. C., Chhabra, P. S., Brooks, W. A., Onasch, T. B., Jayne, J. T., Worsnop, D. R., China, S., Sharma,
471 N., Mazzoleni, C., Xu, L., Ng, N. L., Liu, D., Allan, J. D., Lee, J. D., Fleming, Z. L., Mohr, C., Zotter, P., Szidat,
472 S., and Prévôt, A. S. H.: Enhanced light absorption by mixed source black and brown carbon particles in
473 UK winter, *Nature Communications*, 6, 8435, 10.1038/ncomms9435.
474 <https://www.nature.com/articles/ncomms9435#supplementary-information>, 2015.

475 Liu, Z., Hu, B., Zhang, J., Yu, Y., and Wang, Y.: Characteristics of aerosol size distributions and chemical
476 compositions during wintertime pollution episodes in Beijing, *Atmospheric Research*, 168, 1-12,
477 10.1016/j.atmosres.2015.08.013, 2016.

478 Meng, Z. Y., Ding, G. A., Xu, X. B., Xu, X. D., Yu, H. Q., and Wang, S. F.: Vertical distributions of SO₂ and
479 NO₂ in the lower atmosphere in Beijing urban areas, China, *Sci Total Environ*, 390, 456-465,
480 10.1016/j.scitotenv.2007.10.012, 2008.

481 Merikallio, S., Lindqvist, H., Nousiainen, T., and Kahnert, M.: Modelling light scattering by mineral dust
482 using spheroids: assessment of applicability, *Atmospheric Chemistry and Physics*, 11, 5347-5363,
483 10.5194/acp-11-5347-2011, 2011.

484 Müller, A., Miyazaki, Y., Aggarwal, S. G., Kitamori, Y., Boreddy, S. K. R., and Kawamura, K.: Effects of
485 chemical composition and mixing state on size-resolved hygroscopicity and cloud condensation nuclei
486 activity of submicron aerosols at a suburban site in northern Japan in summer, *Journal of Geophysical*
487 *Research: Atmospheres*, 122, 9301-9318, 10.1002/2017jd027286, 2017.

488 Niu, H., Shao, L., and Zhang, D.: Soot particles at an elevated site in eastern China during the passage of

489 a strong cyclone, *Sci Total Environ*, 430, 217-222, 10.1016/j.scitotenv.2012.04.050, 2012.

490 Niu, H., Hu, W., Zhang, D., Wu, Z., Guo, S., Pian, W., Cheng, W., and Hu, M.: Variations of fine particle
491 physiochemical properties during a heavy haze episode in the winter of Beijing, *Sci Total Environ*, 571,
492 103-109, 10.1016/j.scitotenv.2016.07.147, 2016.

493 Peng, J., Hu, M., Guo, S., Du, Z., Zheng, J., Shang, D., Levy Zamora, M., Zeng, L., Shao, M., Wu, Y. S., Zheng,
494 J., Wang, Y., Glen, C. R., Collins, D. R., Molina, M. J., and Zhang, R.: Markedly enhanced absorption and
495 direct radiative forcing of black carbon under polluted urban environments, *Proc Natl Acad Sci U S A*,
496 113, 4266-4271, 10.1073/pnas.1602310113, 2016.

497 Petaja, T., Jarvi, L., Kerminen, V. M., Ding, A. J., Sun, J. N., Nie, W., Kujansuu, J., Virkkula, A., Yang, X. Q.,
498 Fu, C. B., Zilitinkevich, S., and Kulmala, M.: Enhanced air pollution via aerosol-boundary layer feedback
499 in China, *Sci Rep*, 6, 18998, 10.1038/srep18998, 2016.

500 Platis, A., Altstädter, B., Wehner, B., Wildmann, N., Lampert, A., Hermann, M., Birmili, W., and Bange, J.:
501 An Observational Case Study on the Influence of Atmospheric Boundary-Layer Dynamics on New
502 Particle Formation, *Boundary-Layer Meteorology*, 158, 67-92, 10.1007/s10546-015-0084-y, 2015.

503 Qi, X., Ding, A., Nie, W., Chi, X., Huang, X., Xu, Z., Wang, T., Wang, Z., Wang, J., Sun, P., Zhang, Q., Huo, J.,
504 Wang, D., Bian, Q., Zhou, L., Zhang, Q., Ning, Z., Fei, D., Xiu, G., and Fu, Q.: Direct measurement of new
505 particle formation based on tethered airship around the top of the planetary boundary layer in eastern
506 China, *Atmospheric Environment*, 209, 92-101, 10.1016/j.atmosenv.2019.04.024, 2019.

507 Ramanathan, V., Crutzen, P. J., Mitra, A. P., and Sikka, D.: The Indian Ocean Experiment and the Asian
508 Brown Cloud, *Curr. Sci.*, 83, 947-955, 2002.

509 Rodriguez-Navarro, C., di Lorenzo, F., and Elert, K.: Mineralogy and physicochemical features of Saharan
510 dust wet deposited in the Iberian Peninsula during an extreme red rain event, *Atmospheric Chemistry
511 and Physics*, 18, 10089-10122, 10.5194/acp-18-10089-2018, 2018.

512 Saliba, G., Subramanian, R., Saleh, R., Ahern, A. T., Lipsky, E. M., Tasoglou, A., Sullivan, R. C., Bhandari,
513 J., Mazzoleni, C., and Robinson, A. L.: Optical properties of black carbon in cookstove emissions coated
514 with secondary organic aerosols: Measurements and modeling, *Aerosol Science and Technology*, 50,
515 1264-1276, 10.1080/02786826.2016.1225947, 2016.

516 Scarnato, B. V., Vahidinia, S., Richard, D. T., and Kirchstetter, T. W.: Effects of internal mixing and
517 aggregate morphology on optical properties of black carbon using a discrete dipole approximation
518 model, *Atmospheric Chemistry and Physics*, 13, 5089-5101, 10.5194/acp-13-5089-2013, 2013.

519 Schneider, C. A., Rasband, W. S., and Eliceiri, K. W.: NIH Image to ImageJ: 25 years of image analysis,
520 *Nature Methods*, 9, 671-675, 10.1038/nmeth.2089, 2012.

521 Shao, L., Hou, C., Geng, C., Liu, J., Hu, Y., Wang, J., Jones, T., Zhao, C., and Bérubé, K.: The oxidative
522 potential of PM 10 from coal, briquettes and wood charcoal burnt in an experimental domestic stove,
523 *Atmospheric Environment*, 127, 372-381, 10.1016/j.atmosenv.2015.12.007, 2016.

524 Shao, L., Hu, Y., Shen, R., Schafer, K., Wang, J., Wang, J., Schnelle-Kreis, J., Zimmermann, R., BeruBe, K.,
525 and Suppan, P.: Seasonal variation of particle-induced oxidative potential of airborne particulate matter
526 in Beijing, *Sci Total Environ*, 579, 1152-1160, 10.1016/j.scitotenv.2016.11.094, 2017.

527 Sharma, N., China, S., Bhandari, J., Gorkowski, K., Dubey, M., Zaveri, R. A., and Mazzoleni, C.: Physical
528 Properties of Aerosol Internally Mixed With Soot Particles in a Biogenically Dominated Environment in
529 California, *Geophysical Research Letters*, 45, 11,473-411,482, 10.1029/2018gl079404, 2018.

530 Shi, Z., Vu, T., Kotthaus, S., Harrison, R. M., Grimmond, S., Yue, S., Zhu, T., Lee, J., Han, Y., Demuzere, M.,
531 Dunmore, R. E., Ren, L., Liu, D., Wang, Y., Wild, O., Allan, J., Acton, W. J., Barlow, J., Barratt, B., Beddows,
532 D., Bloss, W. J., Calzolari, G., Carruthers, D., Carslaw, D. C., Chan, Q., Chatzidiakou, L., Chen, Y., Crilley, L.,
533 Coe, H., Dai, T., Doherty, R., Duan, F., Fu, P., Ge, B., Ge, M., Guan, D., Hamilton, J. F., He, K., Heal, M.,
534 Heard, D., Hewitt, C. N., Hollaway, M., Hu, M., Ji, D., Jiang, X., Jones, R., Kalberer, M., Kelly, F. J., Kramer,
535 L., Langford, B., Lin, C., Lewis, A. C., Li, J., Li, W., Liu, H., Liu, J., Loh, M., Lu, K., Lucarelli, F., Mann, G.,
536 McFiggans, G., Miller, M. R., Mills, G., Monk, P., Nemitz, E., amp, apos, Connor, F., Ouyang, B., Palmer, P.
537 I., Percival, C., Popoola, O., Reeves, C., Rickard, A. R., Shao, L., Shi, G., Spracklen, D., Stevenson, D., Sun,
538 Y., Sun, Z., Tao, S., Tong, S., Wang, Q., Wang, W., Wang, X., Wang, X., Wang, Z., Wei, L., Whalley, L., Wu,
539 X., Wu, Z., Xie, P., Yang, F., Zhang, Q., Zhang, Y., Zhang, Y., and Zheng, M.: Introduction to the special
540 issue "In-depth study of air pollution sources and processes within Beijing and its surrounding region
541 (APHH-Beijing)", *Atmospheric Chemistry and Physics*, 19, 7519-7546, 10.5194/acp-19-7519-2019, 2019.

542 Shou, Y., Huang, Y., Zhu, X., Liu, C., Hu, Y., and Wang, H.: A review of the possible associations between
543 ambient PM_{2.5} exposures and the development of Alzheimer's disease, *Ecotoxicol Environ Saf*, 174,
544 344-352, 10.1016/j.ecoenv.2019.02.086, 2019.

545 Sorensen, C.M., 2001. Light Scattering by Fractal Aggregates: A Review. *Aerosol Science and Technology*,
546 35(2): 648-687.

547 Sun, Y., Zhuang, G., Tang, A., Wang, Y., and An, Z.: Chemical Characteristics of PM_{2.5} and PM₁₀ in
548 Haze-Fog Episodes in Beijing, *Environmental Science & Technology*, 40, 3148-3155, 10.1021/es051533g,
549 2006.

550 Sun, Y., Jiang, Q., Wang, Z., Fu, P., Li, J., Yang, T., and Yin, Y.: Investigation of the sources and evolution
551 processes of severe haze pollution in Beijing in January 2013, *Journal of Geophysical Research:*
552 *Atmospheres*, 119, 4380-4398, 10.1002/2014jd021641, 2014.

553 Sun, Y., Du, W., Wang, Q., Zhang, Q., Chen, C., Chen, Y., Chen, Z., Fu, P., Wang, Z., Gao, Z., and Worsnop,
554 D. R.: Real-Time Characterization of Aerosol Particle Composition above the Urban Canopy in Beijing:
555 Insights into the Interactions between the Atmospheric Boundary Layer and Aerosol Chemistry, *Environ*
556 *Sci Technol*, 49, 11340-11347, 10.1021/acs.est.5b02373, 2015.

557 Sun, Y., Du, W., Fu, P., Wang, Q., Li, J., Ge, X., Zhang, Q., Zhu, C., Ren, L., Xu, W., Zhao, J., Han, T., Worsnop,
558 D. R., and Wang, Z.: Primary and secondary aerosols in Beijing in winter: sources, variations and
559 processes, *Atmospheric Chemistry and Physics*, 16, 8309-8329, 10.5194/acp-16-8309-2016, 2016.

560 Sun, Y. L., Wang, Z. F., Fu, P. Q., Yang, T., Jiang, Q., Dong, H. B., Li, J., and Jia, J. J.: Aerosol composition,
561 sources and processes during wintertime in Beijing, China, *Atmospheric Chemistry and Physics*, 13,
562 4577-4592, 10.5194/acp-13-4577-2013, 2013.

563 Tang, M., Czikzo, D. J., and Grassian, V. H.: Interactions of Water with Mineral Dust Aerosol: Water
564 Adsorption, Hygroscopicity, Cloud Condensation, and Ice Nucleation, *Chem Rev*, 116, 4205-4259,
565 10.1021/acs.chemrev.5b00529, 2016.

566 Tao, J., Zhang, L., Cao, J., and Zhang, R.: A review of current knowledge concerning
567 PM_{2.5}; chemical composition, aerosol optical properties and their relationships
568 across China, *Atmospheric Chemistry and Physics*, 17, 9485-9518, 10.5194/acp-17-9485-2017, 2017.

569 Unga, F., Choël, M., Derimian, Y., Deboudt, K., Dubovik, O., and Goloub, P.: Microscopic Observations of
570 Core-Shell Particle Structure and Implications for Atmospheric Aerosol Remote Sensing, *Journal of*
571 *Geophysical Research: Atmospheres*, 123, 13,944-913,962, 10.1029/2018jd028602, 2018.

572 Wang, G., Zhang, R., Gomez, M. E., Yang, L., Levy Zamora, M., Hu, M., Lin, Y., Peng, J., Guo, S., Meng, J.,
573 Li, J., Cheng, C., Hu, T., Ren, Y., Wang, Y., Gao, J., Cao, J., An, Z., Zhou, W., Li, G., Wang, J., Tian, P., Marrero-
574 Ortiz, W., Secretst, J., Du, Z., Zheng, J., Shang, D., Zeng, L., Shao, M., Wang, W., Huang, Y., Wang, Y., Zhu,
575 Y., Li, Y., Hu, J., Pan, B., Cai, L., Cheng, Y., Ji, Y., Zhang, F., Rosenfeld, D., Liss, P. S., Duce, R. A., Kolb, C. E.,
576 and Molina, M. J.: Persistent sulfate formation from London Fog to Chinese haze, *Proc Natl Acad Sci U S*
577 *A*, 113, 13630-13635, 10.1073/pnas.1616540113, 2016.

578 Wang, Q., Sun, Y., Xu, W., Du, W., Zhou, L., Tang, G., Chen, C., Cheng, X., Zhao, X., Ji, D., Han, T., Wang,
579 Z., Li, J., and Wang, Z.: Vertically resolved characteristics of air pollution during two severe winter haze
580 episodes in urban Beijing, China, *Atmospheric Chemistry and Physics*, 18, 2495-2509, 10.5194/acp-18-
581 2495-2018, 2018.

582 Wang, W., Shao, L., Guo, M., Hou, C., Xing, J., and Wu, F.: Physicochemical Properties of Individual
583 Airborne Particles in Beijing during Pollution Periods, *Aerosol and Air Quality Research*, 17, 3209-3219,
584 10.4209/aaqr.2017.03.0116, 2017.

585 Wang, X., Cotter, E., Iyer, K. N., Fang, J., Williams, B. J., and Biswas, P.: Relationship between pyrolysis
586 products and organic aerosols formed during coal combustion, *Proceedings of the Combustion Institute*,
587 35, 2347-2354, 10.1016/j.proci.2014.07.073, 2015.

588 Wang, Y., Yao, L., Wang, L., Liu, Z., Ji, D., Tang, G., Zhang, J., Sun, Y., Hu, B., and Xin, J.: Mechanism for the
589 formation of the January 2013 heavy haze pollution episode over central and eastern China, *Science*
590 *China Earth Sciences*, 57, 14-25, 10.1007/s11430-013-4773-4, 2013.

591 Wehner, B., Siebert, H., Ansmann, A., Ditas, F., Seifert, P., Stratmann, F., Wiedensohler, A., Apituley, A.,
592 Shaw, R. A., Manninen, H. E., and Kulmala, M.: Observations of turbulence-induced new particle
593 formation in the residual layer, *Atmospheric Chemistry and Physics*, 10, 4319-4330, 10.5194/acp-10-
594 4319-2010, 2010.

595 Li, W., Xu, L., Liu, X., Zhang, J., Lin, Y., Yao, X., Gao, H., Zhang, D., Chen, J., Wang, W., Harrison, R. M.,
596 Zhang, X., Shao, L., Fu, P., Athanasios Nenes, and Zongbo Shi: Air pollution–aerosol interactions produce
597 more bioavailable iron for ocean ecosystems, *Science Advance*, 3, e1601749, 2017.

598 Xia, Y., Guan, D., Meng, J., Li, Y., and Shan, Y.: Assessment of the pollution–health–economics nexus in
599 China, *Atmospheric Chemistry and Physics*, 18, 14433-14443, 10.5194/acp-18-14433-2018, 2018.

600 Xu, L., Liu, L., Zhang, J., Zhang, Y., Ren, Y., Wang, X., and Li, W.: Morphology, Composition, and Mixing
601 State of Individual Aerosol Particles in Northeast China during Wintertime, *Atmosphere*, 8,
602 10.3390/atmos8030047, 2017.

603 Xu, L., Zhang, D., and Li, W.: Microscopic comparison of aerosol particles collected at an urban site in
604 North China and a coastal site in Japan, *Sci Total Environ*, 669, 948-954, 10.1016/j.scitotenv.2019.03.163,

605 2019.

606 Yuan, Q., Li, W., Zhou, S., Yang, L., Chi, J., Sui, X., and Wang, W.: Integrated evaluation of aerosols during
607 haze-fog episodes at one regional background site in North China Plain, *Atmospheric Research*, 156,
608 102-110, 10.1016/j.atmosres.2015.01.002, 2015.

609 Zhang, D., Chen, B., Yamada, M., Niu, H., Wang, B., Iwasaka, Y., and Shi, G.: Elevated soot layer in polluted
610 atmosphere: A case study in Beijing, *Journal of the Meteorological Society of Japan.*, 90, 361-375,
611 10.2151/jmsj.2012-302, 2012.

612 Zhang, J., Liu, L., Wang, Y., Ren, Y., Wang, X., Shi, Z., Zhang, D., Che, H., Zhao, H., Liu, Y., Niu, H., Chen, J.,
613 Zhang, X., Lingaswamy, A. P., Wang, Z., and Li, W.: Chemical composition, source, and process of urban
614 aerosols during winter haze formation in Northeast China, *Environ Pollut*, 231, 357-366,
615 10.1016/j.envpol.2017.07.102, 2017.

616 Zhang, J., Liu, L., Xu, L., Lin, Q., Zhao, H., Wang, Z., Guo, S., Hu, M., Liu, D., Shi, Z., Huang, D., and Li, W.:
617 Exploring wintertime regional haze in northeast China: role of coal and biomass burning, *Atmos. Chem.*
618 *Phys.*, 20, 5355-5372, 10.5194/acp-20-5355-2020, 2020.

619 Zhang, Q., Ma, X., Tie, X., Huang, M., and Zhao, C.: Vertical distributions of aerosols under different
620 weather conditions: Analysis of in-situ aircraft measurements in Beijing, China, *Atmospheric*
621 *Environment*, 43, 5526-5535, <https://doi.org/10.1016/j.atmosenv.2009.05.037>, 2009.

622 Zhou, W., Sun, Y., Xu, W., Zhao, X., Wang, Q., Tang, G., Zhou, L., Chen, C., Du, W., Zhao, J., Xie, C., Fu, P.,
623 and Wang, Z.: Vertical Characterization of Aerosol Particle Composition in Beijing, China: Insights From
624 3 - Month Measurements With Two Aerosol Mass Spectrometers, *Journal of Geophysical Research:*
625 *Atmospheres*, 123, 13,016-013,029, 10.1029/2018jd029337, 2018a.

626 Zhou, W., Wang, Q., Zhao, X., Xu, W., Chen, C., Du, W., Zhao, J., Canonaco, F., Prévôt, A. S. H., Fu, P.,
627 Wang, Z., Worsnop, D. R., and Sun, Y.: Characterization and source apportionment of organic aerosol at
628 260 m on a meteorological tower in Beijing, China, *Atmospheric Chemistry and Physics*, 18,
629 3951-3968, 10.5194/acp-18-3951-2018, 2018b.

630 Zhu, J., Crozier, P. A., and Anderson, J. R.: Characterization of light-absorbing carbon particles at three
631 altitudes in East Asian outflow by transmission electron microscopy, *Atmospheric Chemistry and Physics*,
632 13, 6359-6371, 10.5194/acp-13-6359-2013, 2013.

633

634 Table 1 Sample information and meteorological conditions

Sample ID ^①	Date (2016)	Time ^②	PM _{2.5} ($\mu\text{g m}^{-3}$)	SO ₂ ($\mu\text{g m}^{-3}$)	NO ₂ ($\mu\text{g m}^{-3}$)	O ₃ ($\mu\text{g m}^{-3}$)	RH (%)	T (°C)	MLH (m) ^③
Z1-1	12/1	9:10	12 ^④	2	48	37	24	6	--
Z2-1	12/1	8:40	--	--	--	--	--	--	194
Z1-2	12/2	1:00	110	25	109	3	55	2	--
Z2-2	12/2	1:00	--	--	--	--	--	--	141
Z1-3	12/2	9:10	24	20	134	2	50	3	--
Z2-3	12/2	8:40	--	--	--	--	--	--	134
Z1-4	12/3	1:53	142	36	102	6	79	-1	--
Z2-4	12/3	3:00	--	--	--	--	--	--	232
Z1-5	12/4	1:04	530	14	180	4	93	1	--
Z2-5	12/4	3:00	--	--	--	--	--	--	136
Z1-6	12/5	2:00	86	8	21	53	75	2	--
Z2-6	12/5	2:00	--	--	--	--	--	--	114
Z1-7	12/8	9:10	187	2	16	72	86	2	--
Z2-7	12/8	8:40	--	--	--	--	--	--	191
Z1-8	12/9	9:20	12	8	67	12	33	2	--
Z2-8	12/9	8:30	--	--	--	--	--	--	250

635 ① Samples are collected at two altitudes: Z1 is 2 m above ground and Z2 is 280 m above ground.

636 ② Sampling duration ranges from 30 seconds to less than 5 minutes depending on the PM pollution.

637 ③ MLH represents the mixed layer height and the data are 15minutes average; MLH is less than
638 280 m and the samples collected at Z2 represent samples above the mixed layer. ④ If PM_{2.5} mass639 concentration is less than 75 $\mu\text{g m}^{-3}$, samples are classified as non-haze samples and if PM_{2.5} mass640 concentration is more than 75 $\mu\text{g m}^{-3}$, samples are classified as haze samples.

641

642 Table 2 Classification and characteristics of individual particle types.

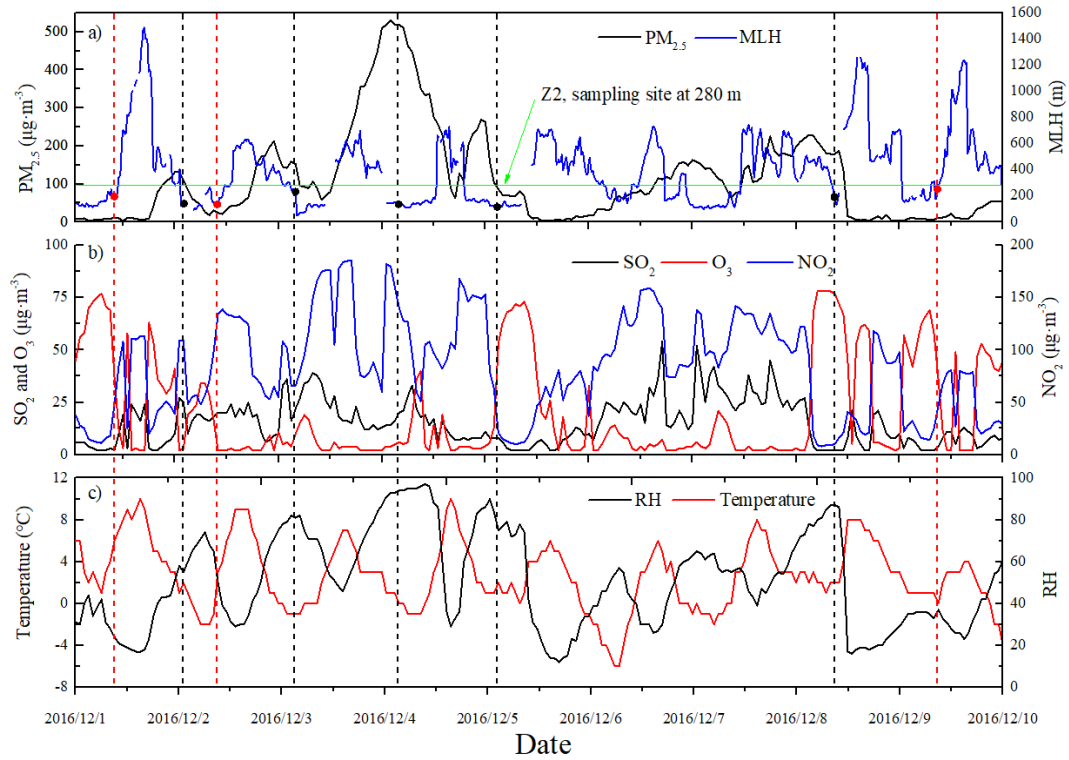
Particle type	Elemental composition	Morphology	Possible sources
Soot particles	C and minor amounts of O, Si.	Chain-like or compact C-dominated aggregates.	Incomplete combustion of biomass and fossil fuel.
Primary organic particles	C and O with minor amounts of Si, K, S, Cl.	Spherical, near spherical or irregular shapes.	Mainly from Combustion process of biomass and fossil fuels.
Mineral particles	O, Si, Al, Ca, Fe, Na, K, Mg, Ti, and S.	Irregular shapes.	Re-suspended from soil dust, road dust, and construction dust.
Metal particles	Fe, Zn, Mn, Ti, and Pb.	Spherical or irregular shapes.	Industries, coal-fired power plants and oil refineries.
S-rich particles	S and O with minor amounts of N, K.	Spherical, near spherical or irregular shapes.	Secondary aerosol formation.
Organic mixed with Sulfur-rich particles	C, O, and S with minor amounts of N, K or Cl.	Irregular shapes.	Secondary aerosol reaction.
Other mixed particles	Complex elemental composition.	Irregular shapes with different particle types.	Secondary aerosol reaction.

643

644 Table 3 Relative number percentage of individual particles.

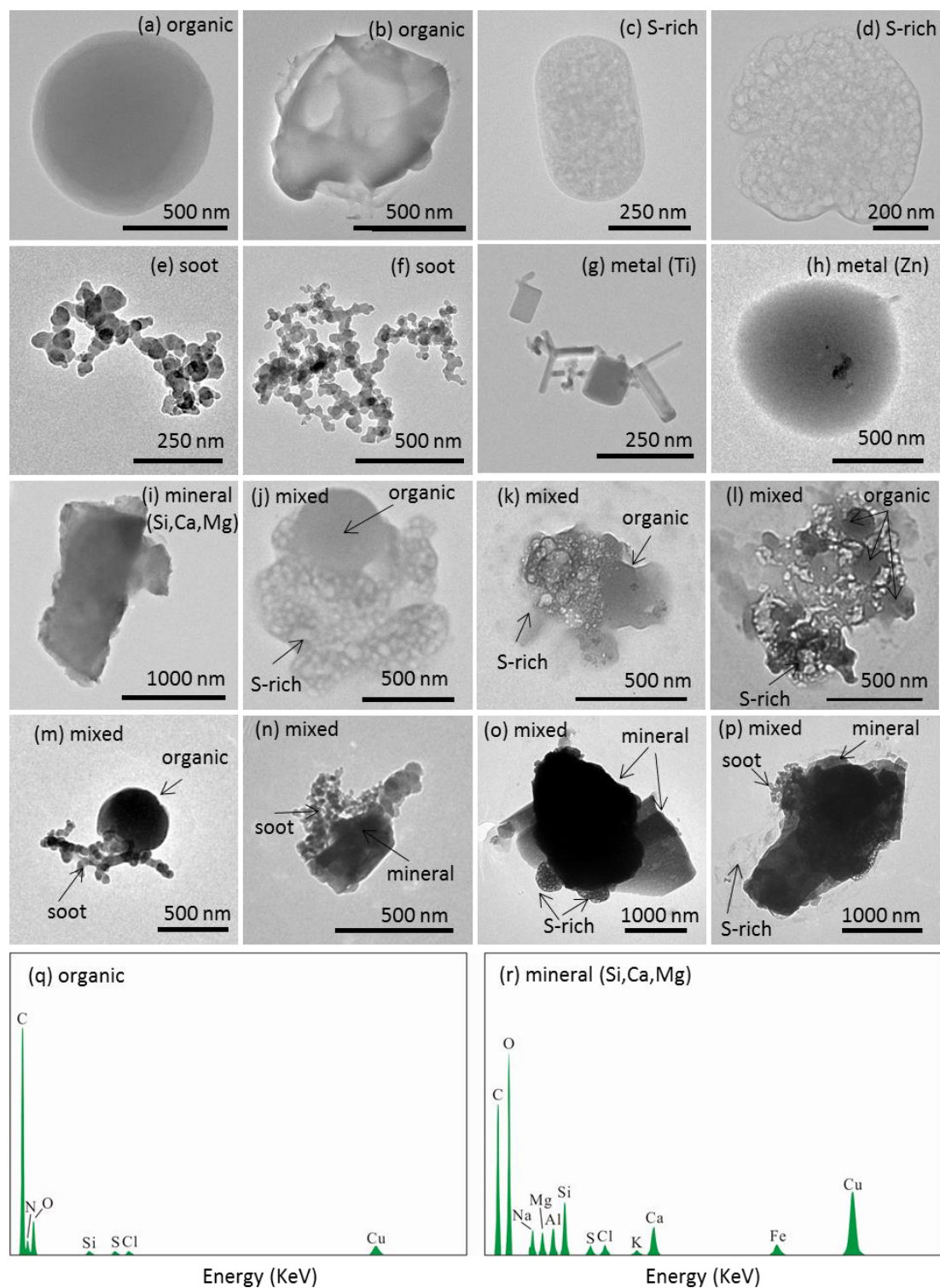
Air qualities	Sample ID	Number	Metals	Minerals	POA	S-rich	Soot	OP-S	Other
Non-haze periods	Z1-1	114	2.6	30.7	19.3	36.0	5.3	1.8	4.4
	Z2-1	113	1.8	12.4	16.8	56.6	10.6	0.9	0.9
	Z1-3	135	4.4	34.1	31.9	12.6	11.1	0.7	5.2
	Z2-3	118	2.5	23.7	45.8	17.0	4.2	2.5	4.2
	Z1-8	140	1.4	62.9	12.1	11.4	2.9	2.1	7.1
	Z2-8	119	3.4	33.6	19.3	18.5	17.7	0.0	7.6
	Ave (Z1)	389	2.8	42.5	21.1	20.0	6.4	1.6	5.6
	Ave (Z2)	350	2.6	23.2	27.3	30.7	10.8	1.1	4.2
Haze periods	Z1-2	123	2.4	21.1	42.3	17.1	7.3	2.4	7.3
	Z2-2	164	4.9	14.6	37.2	25.0	4.3	9.8	4.3
	Z1-4	160	0.6	28.8	30.6	8.8	13.8	9.4	8.1
	Z2-4	266	0.0	3.8	53.0	3.4	7.1	19.6	13.2
	Z1-5	461	0.9	6.5	18.9	22.1	7.6	31.5	12.6
	Z2-5	266	0.4	0.4	32.3	7.1	2.3	44.0	13.5
	Z1-6	237	2.5	11.0	21.5	48.5	2.1	6.8	7.6
	Z2-6	281	1.8	11.0	18.9	19.6	12.8	15.3	20.6
	Z1-7	168	1.8	23.2	28.0	20.8	2.4	15.5	8.3
	Z2-7	192	1.6	17.7	32.3	27.1	1.6	15.1	4.7
	Ave (Z1)	1149	1.7	18.1	28.3	23.5	6.6	13.1	8.8
	Ave (Z2)	1169	1.7	9.5	34.7	16.4	5.6	20.7	11.3

645



646

647 Fig. 1: The dashed lines represent the individual particle sampling times with red lines representing
 648 non-haze samples and black lines haze samples. (a) Temporal variations of mixed layer height
 649 (MLH) and $PM_{2.5}$ mass concentrations. The solid dots represent the MLH during the sampling times.
 650 (b) Temporal variations of SO_2 , NO_2 , O_3 at ground level at the Olympic Park monitor site, which is
 651 the closest national air quality monitor station to the sampling site (~1.5 km). (c) Temporal variations
 652 of temperature (T) and relative humidity (RH) at ground level. Date was obtained from the Ministry
 653 of Ecology and Environment of China (<https://www.aqistudy.cn>).
 654



655

656

657

658

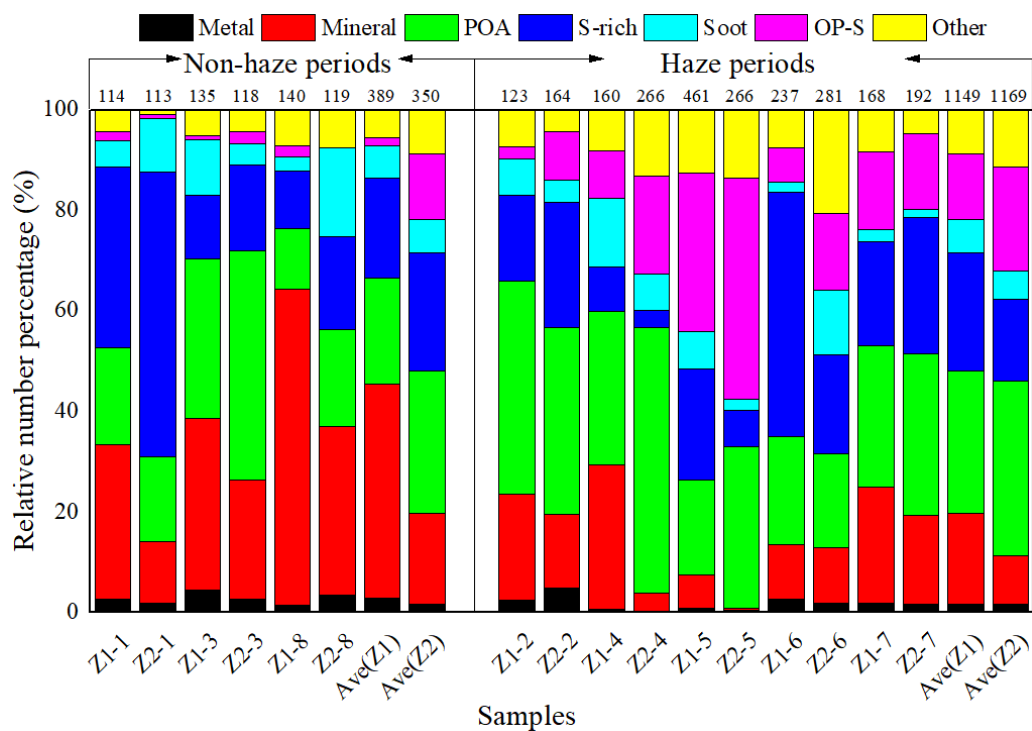
659

660

661

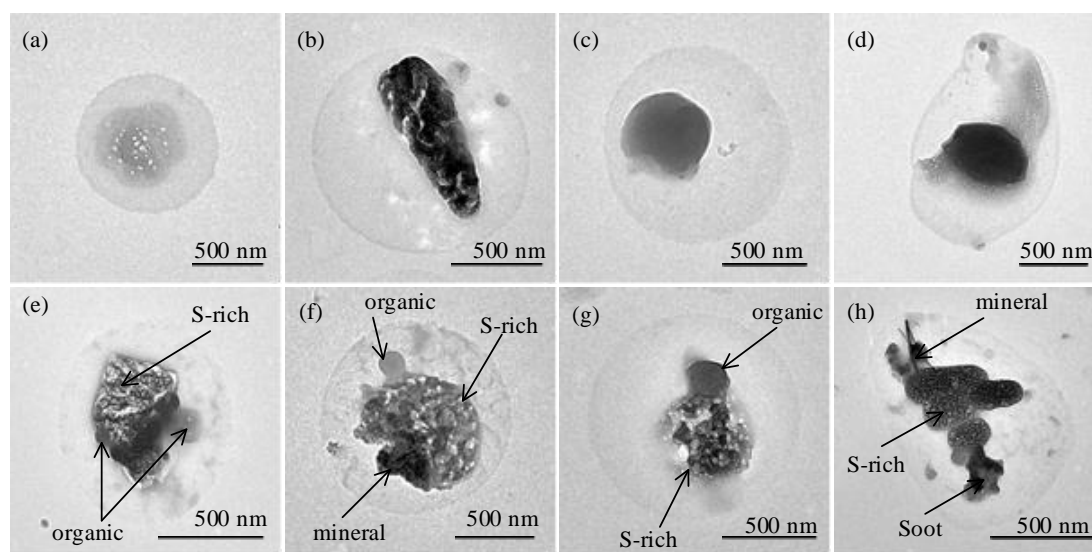
662

Fig. 2: Examples of morphologies and mixing characteristics of individual aerosol particles in winter in Beijing at ground level and above the mixed layer. (a) Spherical organic particle, (b) irregular shaped organic particle, (c-d) S-rich particles, (e-f) soot particles, (g-h) metal particles, (i) mineral particles, (j-l) OP-S mixed particles, and (m-p) other mixed particle types. (q) and (r) are EDS of (b) and (i). The difference between the particles in (b) and (i) is that organic particles (b) mainly composed C and O while minerals (i) mainly composed O, Si, Ca and Mg.



664

665 Fig. 3: Relative number percentage of different particle types at ground level (Z1) and above the
 666 mixed layer height (Z2). The number above each bar represents the total particle number analyzed
 667 in each sample.

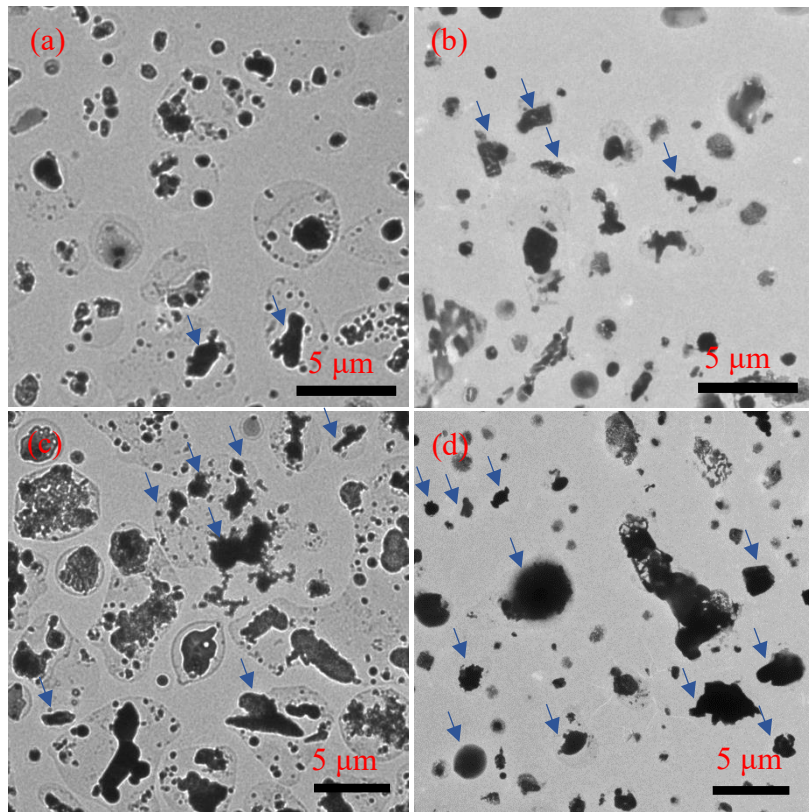


669

670

671

Fig. 4: Images of core-shell structured particles. (a-b) S-rich cores, (c-d) organic cores, and (e-h) mixed cores.



672

673

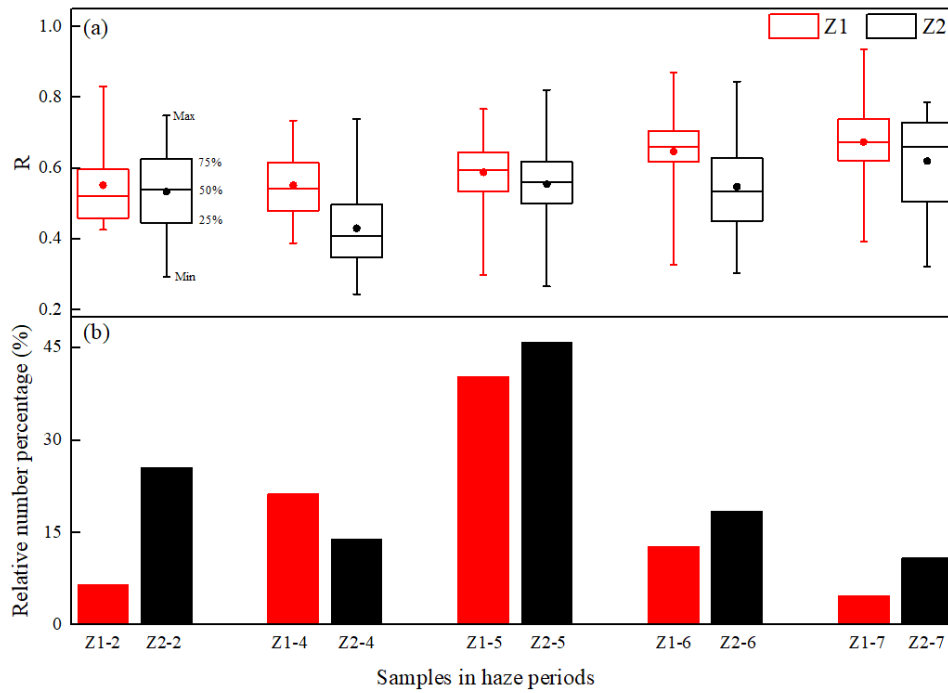
674

675

676

677

Fig. 5: Low magnification images of individual particles. (a) and (c) are particles above the mixed layer (MLH) at different size ranges. (b) and (d) are particles at ground level at different size ranges. More coated particles were found above the MLH. Arrows show part of the mineral particles.



678

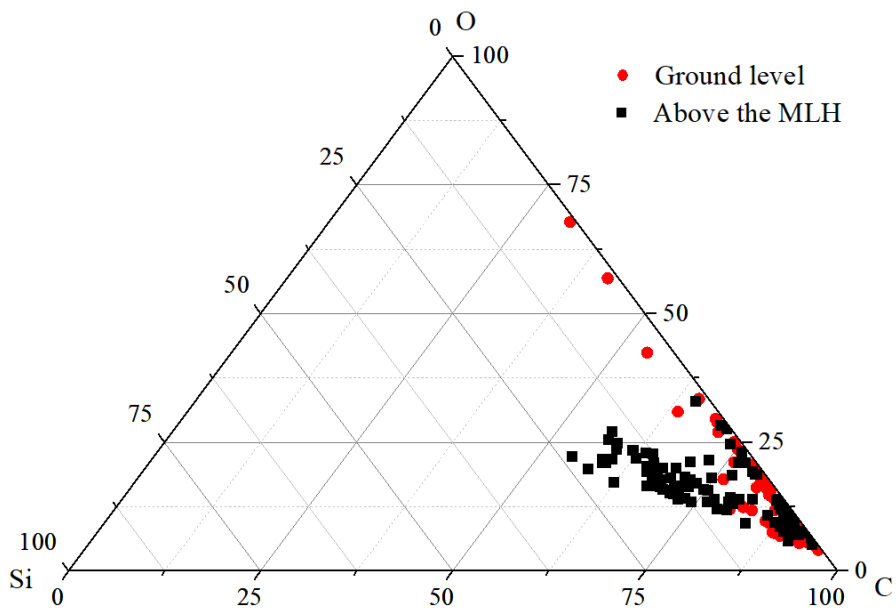
679

680

681

682

Fig. 6: (a) R is C/S ratio (D_{Aeq} ratio of the core to the whole particle including the shell) of particles during haze periods at ground level (Z1) and above the mixed layer height (Z2); solid dots represent the average value, and (b) the corresponding relative number percentage of core-shell structured particles.



683
 684
 685
 686

Fig. 7: Triangular diagram showing the weight ratio of C-O-Si of primary organic aerosols (POA) at ground level and above the mixed layer height (MLH).